Journal of Neurochemistry

WILEY

Journal of Neurochemistry JNC The Official Journal of the International Society for Neurochemistry

ORIGINAL ARTICLE

Tubulin-Binding Region Modulates Cholesterol-Triggered Aggregation of Tau Proteins

Abid Ali | Mikhail Matveyenka | Davis N. Pickett | Axell Rodriguez | Dmitry Kurouski

Department of Biochemistry and Biophysics, Texas A&M University, College Station, Texas, USA

Correspondence: Dmitry Kurouski (dkurouski@tamu.edu)

Received: 19 September 2024 | **Revised:** 4 December 2024 | **Accepted:** 11 December 2024

Funding: This work was supported by NIGMS (R35GM142869).

Keywords: amyloids | cholesterol | fibrils | Tau

ABSTRACT

A hallmark of Alzheimer disease (AD) and tauopathies, severe neurodegenerative diseases, is the progressive aggregation of Tau, also known as microtubule-associated Tau protein. Full-length $Tau_{1\text{-}441}$, also known as 2N4R, contains two N-terminal inserts that bind to tubulin. This facilitates the self-assembly of tubulin simultaneously enhancing stability of cell microtubules. Other Tau isoforms have one (1N4R) or zero (0N4R) N-terminal inserts, which makes 2N4R Tau more and 0N4R less effective in promoting microtubule self-assembly. A growing body of evidence indicates that lipids can alter the aggregation rate of Tau isoforms. However, the role of N-terminal inserts in Tau-lipid interactions remains unclear. In this study, we utilized a set of biophysical methods to determine the extent to which N-terminal inserts alter interactions of Tau isoforms with cholesterol, one of the most important lipids in plasma membranes. Our results showed that 2N insert prevents amyloid-driven aggregation of Tau at the physiological concentration of cholesterol, while the absence of this N-terminal repeat (1N4R and 0N4R Tau) resulted in the self-assembly of Tau into toxic amyloid fibrils. We also found that the presence of cholesterol in the lipid bilayers caused a significant increase in the cytotoxicity of 1N4R and 0N4R Tau to neurons. This effect was not observed for 2N4R Tau fibrils formed in the presence of lipid membranes with low, physiological, and elevated concentrations of cholesterol. Using molecular assays, we found that Tau aggregates primarily exert cytotoxicity by damaging cell endosomes, endoplasmic reticulum, and mitochondria.

1 | Introduction

Tauopathies, including progressive supranuclear palsy and frontotemporal dementia, are severe diseases that are linked to the self-assembly of Tau proteins (Ait-Bouziad et al. 2017; Alonso Adel et al. 2004; Asai et al. 2015; Clavaguera et al. 2009). A hallmark of these pathologies is a profound neuronal loss in the frontal part of the brain (Takashima 2013; Yoshiyama et al. 2007; Zhang et al. 2019). Although the exact cause of tauopathies remains unclear, the neuronal loss is linked to the formation and spread of Tau oligomers and fibrils. These toxic β-sheet–rich aggregates exhibit high structural and morphological variability (Eisenberg and Sawaya 2017; Falcon et al. 2019; Gerson et al. 2016; Grundke-Iqbal et al. 1986; Hoshi et al. 2003). Similar aggregates were observed upon histological analysis of patients diagnosed with Alzheimer disease (AD) (Takashima 2013; Ait-Bouziad et al. 2017; Lasagna-Reeves et al. 2012a; Zempel et al. 2010). In addition to extracellular amyloid plaques that are dominated by amyloid β-fibrils, AD is characterized by the development of neurofibrillary tangles.

Abbreviations: AD, Alzheimer disease; AFM, atomic force microscopy; AFM-IR, atomic force microscopy–infrared spectroscopy; ATF6, activating transcription factor 6; Cho, cholesterol; DMPC, 1,2-dimyristoyl-sn-glycero-3-phosphocholine; FTIR, Fourier-transformed infrared spectroscopy; GRP78, glucose-regulated chaperon; LUVs, large unilamellar vesicles; PBS, phosphate buffer saline; PERK, protein endoplasmic reticulum kinase; PMSF, phenylmethylsulfonyl fluoride; PS, phosphatidylserine; QCL, quantum-cascade laser; $t_{1/2}$, half-time; ThT, thioflavin T; t_{lag}, lag-time; TTR, transthyretin; UPR, unfolded protein response; XBP-1, X-box binding protein 1.

These intracellular formations contain aggregates of hyperphosphorylated Tau (Takashima 2013; Wang et al. 2017; Wegmann et al. 2018; Yoshiyama et al. 2007).

Tau proteins play an important role in polymerization and stabilization of microtubules in neurons (McLean et al. 1999; Gouras et al. 2010). Tau isoforms are expressed as a result of alternative splicing of exons 2, 3, and 10 (Goedert et al. 1989; Himmler et al. 1989). Full-length $Tau_{1\text{-}441}$, also known as 2N4R, contains two N-terminal inserts that determine Tau binding to tubulin, a building block of the cell microtubules (Weingarten et al. 1975; Grundke-Iqbal et al. 1986). Tau isoforms may also have one (1N4R) and zero (0N4R) N-terminal inserts. Consequently, 2N4R Tau becomes more and 0N4R less effective in promoting microtubule self-assembly (Alonso Adel et al. 2004; Alonso et al. 2001). In the presence of glycosaminoglycan heparin, Tau isoforms can aggregate forming cytotoxic amyloid oligomers and fibrils (Giamblanco et al. 2020; Falcon et al. 2019; Zhang et al. 2019). These protein aggregates exhibit high morphological and structural heterogeneity (Takashima 2013; Lasagna-Reeves et al. 2012b; Karikari et al. 2019; Eisenberg and Sawaya 2017; Shafiei, Guerrero-Munoz, and Castillo-Carranza 2017). It was demonstrated that injection of Tau oligomers into mice's brains caused cognitive, synaptic, and mitochondrial abnormalities. Such symptoms were not observed upon the injections of Tau monomers (Lasagna-Reeves, Castillo-Carranza, Jackson et al. 2011; Lasagna-Reeves, Castillo-Carranza, Sengupta et al. 2011). The pathological progression of tauopathies and AD have been linked to anatomically connected neurons (Nath et al. 2012; Rajendran et al. 2006; Wang et al. 2017). The cell-to-cell transfer of Tau aggregates has been demonstrated in in vitro neuronal models (Clavaguera et al. 2009; Nath et al. 2012). Specifically, Tau oligomers exhibited fast axonal transport in the anterograde direction at all physiological Tau levels (LaPointe et al. 2009; Morfini et al. 2009).

Dicke et al. (2017) utilized PC 1,2-dioleoyl-sn-glycero-3-pho sphocholine:1,2-dioleoyl-sn-glycero-3-phospho-(10-rac-glycerol) vesicles to determine Tau region that interacts with lipids. For this, each R domain (R1, R2, R3, and R4) was isolated and tested using isothermal titration calorimetry. It was found that R2 and R3 domains exhibited the strongest interactions with lipid vesicles. However, it remained unclear whether such interactions could be expected in the N terminus of the protein (Elbaum-Garfinkle, Ramlall, and Rhoades 2010; Sallaberry et al. 2021). Expanding upon this, our group recently investigated the role of 2 N insert in Tau binding to anionic lipids. Ali et al. 2024 found that the rate of aggregation of 2N4R Tau isoform could be altered by the length and saturation of fatty acids in phosphatidylserine (PS), anionic lipid that is primarily localized on the inner part of plasma membranes. However, this effect was not observed for 1N4R Tau (Ali et al. 2024). These results indicate that 2 N insert plays a critically important role in protein–lipid interactions. Ait-Bouziad et al. 2017 demonstrated that not only 2N4R but also K18 isoform could interact with PS. This results in the formation of highly toxic oligomers (Ait-Bouziad et al. 2017). NMR revealed that Tau and lipids in such oligomers were stabilized by strong electrostatic interactions between the charged amino acid residues of Tau and polar heads of PS (Ait-Bouziad et al. 2017). Yau and coworkers found that not only the presence of PS but also the protein-to-lipid ratio strongly influenced the secondary structure of Tau-lipid oligomers (Yao et al. 2022).

Recently reported results by Zhaliazka, Matveyenka, and Kurouski 2023 showed that cholesterol could drastically accelerate the aggregation rate of amyloid $\beta_{1\text{-}42}$ peptide. Similar findings were reported by (Ali, Zhaliazka, Dou, Holman, Kumar et al. 2023; Ali et al. 2023a, 2023b) for transthyretin (TTR), a hormone that transports thyroxine. Specifically, low concentrations of cholesterol decelerated the aggregation of TTR, whereas high concentrations of these lipids triggered nearly instantaneous protein self-assembly (Ali et al. 2023a). Nevertheless, TTR fibrils formed in the presence of cholesterol at different concentrations exerted similar levels of cytotoxicity which was lower compared to the cytotoxicity of TTR fibrils formed in the lipid-free environment. Furthermore, Jakubec et al. (2021) found that cholesterol uniquely alters the binding efficiency of α-synuclein (α-syn), a small protein that is linked to the onset and spread of Parkinson disease, to lipid bilayers. Furthermore, the researchers observed different strengths of α-syn–membrane interactions at different cholesterol concentrations (Jakubec et al. 2021).

Expanding upon this, we investigated the effects of large unilamellar vesicles (LUVs) composed of low (10%), physiological (45%), and elevated (60%) concentrations of cholesterol on the aggregation rate of 0N4R, 1N4R, and 2N4R Tau isoforms. We also utilized biophysical techniques to examine changes in the morphologies and secondary structure of protein aggregates formed under these conditions, as well as cytotoxicity of 0N4R, 1N4R, and 2N4R Tau fibrils formed at low, physiological, and elevated concentrations of cholesterol. Finally, we used a set of cell and molecular assays to determine mechanisms by which such protein aggregates exert cytotoxicity in neurons.

2 | Methods

2.1 | Experimental Section

2.1.1 | Materials

1,2-Dimyristoyl-sn-glycero-3-phosphocholine (DMPC or PC) (Catalog No. 850345P-25 mg) and cholesterol (Catalog No. 700100P-100 mg) were purchased from Avanti (Alabaster, AL, USA) https://avantiresearch.com; IPTG from Sigma-Aldrich (Catalog No. I6758) (St. Louis, MO, USA) www.sigmaaldrich.com; urea was purchased from Sigma-Aldrich (Catalog No. 57–13-6) (St. Louis, MO, USA) www.sigmaaldrich.com; Tris was purchased from BIO-RAD (Catalog No. 161 071); NaCl from Sigma-Aldrich (Catalog No. S9625) (St. Louis, MO, USA) www.sigmaaldrich.com; DTT from Sigma-Aldrich (Catalog No. 3483-12-3) (St. Louis, MO, USA) www.sigmaaldrich.com; β-mercaptoethanol (BME) (Catalog No. 21985023) from Thermos Scientific www.thermofisher.com; phenylmethylsulfonyl fluoride (PMSF) from Sigma-Aldrich (Catalog No. P7626) (St. Louis, MO, USA) www.sigmaaldrich.com; imidazole from Sigma-Aldrich (Catalog No. 288–32-4) (St. Louis, MO, USA); and Ni-NTA agarose beads from Fisher Scientific (Catalog No. R90115) www.fishersci.com.

2.1.2 | Liposome Preparation

LUVs of PC and cholesterol were prepared according to the procedure reported by Mateyenka and coworkers (Matveyenka, Rizevsky, and Kurouski 2022; Matveyenka et al. 2023, 2022). Lipids at various molar ratios were initially dissolved in chloroform. After the solvent was completely evaporated, the resulting lipid film was rehydrated in PBS at pH 7.4. LUVs with a target diameter of ~100 nm were then prepared using a freeze–thaw cycle. The lipid suspensions were first heated to 50°C for 30 min, followed by rapid freezing in liquid nitrogen for 3–5 min. Subsequently, the lipid solutions were subjected to an extrusion process, where they were passed 20–30 times through a 100-nm polycarbonate membrane (Catalog No. 610005-1EA) (Avanti, Alabaster, AL, USA). The size of the LUVs was determined by dynamic light scattering, and all samples exhibited an average diameter of 100 ± 10 nm.

2.2 | Protein Expression and Purification of 0N4R, 1N4R, and 2N4R Tau

The proteins pET28b-Tau 2N4R, pET28b-Tau 1N4R, and pET28b-Tau 0N4R were overexpressed in *Escherichia coli* BL21 (DE3). Rosetta strain from Sigma-Aldrich (Catalog No.70954) (St. Louis, MO, USA) www.sigmaaldrich.com using LB broth. A total of 8 L of bacterial culture was grown to an optical density (OD600) of 0.9, at which point protein expression was induced by adding 1 mM isopropyl β-D-1-thiogalactopyranoside (IPTG). The cultures were incubated overnight at 16°C. After the induction period, the cultures were harvested by centrifugation at 8000 RPM for 10 min to collect the cell pellets.

The pellets were resuspended in a lysis buffer containing 8 M urea, 50 mM Tris–HCl, 50 mM NaCl, pH 8.0, 1 mM DTT, 1 mM BME, and a protease inhibitor cocktail, including 100 mM PMSF. The resuspended cells underwent a freeze–thaw cycle followed by sonication at 28% amplitude. The lysates were then centrifuged at 16 000 g for 1 h to separate the soluble fraction, and the supernatants were collected. To remove any remaining particulates, the supernatants were filtered through a 0.4-μm syringe filter. The filtered supernatants were subjected to affinity chromatography using Ni-NTA agarose beads in a gravity-flow column. The column was extensively washed with a buffer containing 50 mM Tris–HCl, 300 mM NaCl, and 20 mM imidazole to remove nonspecifically bound proteins. The target proteins were eluted using a buffer composed of 50 mM Tris–HCl, 300 mM NaCl, and 300 mM imidazole, with a total elution volume of 50 mL.

The eluted proteins were dialyzed against PBS (pH 7.4) using a 30 kDa molecular weight cut-off (MWCO) dialysis membrane from Fisher Scientific (Catalog no. 88242) www.fishersci.com to remove urea and imidazole. Postdialysis, the protein samples were concentrated using centrifugal concentrators with a 30 kDa MWCO. The final concentration of the purified proteins was approximately 2.5 mg/mL.

The N-terminal His tag was cleaved using thrombin protease at a ratio of 2 units per milligram of protein, with overnight incubation at 4°C in a dialysis bag. Following cleavage, the protein was concentrated using Centricon centrifugal filter units with a 10 kDa MWCO. To remove residual His tags and thrombin, the concentrated protein was subjected to a second purification step using Ni-NTA and heparin agarose beads in gravity flow columns. This ensures the final preparation is free from both the His tag and protease contaminants (Figure S1).

2.2.1 | 0N4R, 1N4R, and 2N4R Tau Aggregation

In a lipid-free environment, 50 μM of protein was dissolved in PBS, and the solution was adjusted to pH 7.4. For the aggregation of 0N4R, 1N4R, and 2N4R Tau in the presence of LUVs, 50 μM of protein was mixed with the corresponding lipid vesicles at a 1:2 protein-to-lipid molar ratio, and the pH of the final solution was adjusted to pH 7.4 using concentrated HCl. Next, 12.5 μM heparin was used to aggregate the protein. The samples were then transferred to a 96-well plate and incubated in a plate reader (Tecan, Männedorf, Switzerland) at 37°C with agitation at 510 rpm for 350 h. To ensure the absence of protein degradation for 350 h, SDS gel was permitted (Figure S2).

2.2.2 | Kinetic Measurements

Protein aggregation rates were assessed using a thioflavin T (ThT) fluorescence assay. For the assay, samples were mixed with a 25 μM ThT solution and transferred to a 96-well plate. The plate was then placed in a Tecan plate reader (Männedorf, Switzerland) and incubated at 37°C for 350 h with continuous agitation at 510 rpm. Fluorescence measurements were recorded every 15 min with an excitation wavelength of 450 nm and an emission wavelength of 488 nm. Each kinetic curve represents an average of four independent measurements. One-way ANOVA followed by Tukey's HSD test was used to determine statistical significance of the data (Table 1).

TABLE 1 | Statistical analysis results of experimental data.

	***F* (DFn, DFd)**	***p***
Figure 1 t_{lag}	$F(7, 17) = 65.23$	< 0.0001
Figure 1 $t_{1/2}$	$F(7, 17) = 74.63$	< 0.0001
Figure 6A	$F(5, 12) = 281.8$	< 0.0001
Figure 6B	$F(5, 12) = 173.9$	< 0.0001
Figure 6C	$F(5, 12) = 151.1$	< 0.0001
Figure 6D	$F(4, 10) = 28.92$	< 0.0001
Figure 7A	$F(19, 200) = 25.27$	< 0.0001
Figure 7B	$F(19, 200) = 86.72$	< 0.0001
Figure 9A	$F(5, 10) = 112.9$	< 0.0001
Figure 9B	$F(5, 12) = 78.19$	< 0.0001
Figure 9C	$F(5, 12) = 85.89$	< 0.0001
Figure 9D	$F(4, 10) = 21.81$	< 0.0001

2.2.3 | Atomic Force Microscopy (AFM) Imaging

AIST-NT-HORIBA system (Edison, NJ) AFM system was utilized to perform topological characterization of Tau aggregates. Tapping-mode AFM probes (Appnano, Mountain View, CA, USA) were used with force constant of 2.7 N/m and resonance frequency of 50–80 kHz. Sample was first diluted with DI water and then placed on the surface of precleaned glass coverslip. Preprocessing of the collected AFM images was made using AIST-NT software (Edison, NJ, USA).

2.2.4 | AFM-Infrared Spectroscopy (AFM-IR)

Protein samples were deposited onto a 70-nm gold-coated silicon wafer at a volume of 3–6 μL. The deposited sample was left to dry at room temperature for 15–20 min, then rinsed with DI water, and lastly, dried with an N_2 airflow. AFM-IR imaging and spectral acquisition were acquired using a nanoIR3 system (Bruker, Santa Barbara, CA, USA), equipped with a QCL laser. AFM imaging was collected through contact mode using ContGB-G AFM probes (NanoAndMore). The contact-mode tip was optimized using a polymethyl acrylate standard sample for the following wavenumbers: 1400–1800 cm^{-1}. Laser parameters for 0N4R include a starting power of 18.55%, polarization at 90 deg., an averaged pulse rate of 820 kHz, and an IR focus at 52 833 pt. Parameters for 1N4R include a starting power of 25.49%, an average pulse rate of 820 kHz, and an IR focus at 70 249 pt. Lastly, 2N4R parameters include a starting power of 18.55%, an averaged pulse rate at 200 kHz, and an IR focus at 54 500 pt. Differences in pulse rate, power, and IR focus will vary on factors such as AFM probes, sample density, humidity, and external vibrations. Images were taken at a scan rate of 0.3 to 0.8 Hz with a height and width ranging from 1 to 10 μm, resolution of 256 for both X and Y parameters, and an I and P gain of 2 and 4, respectively. An average of 30 spectra were collected per sample with a co-average of 3 for each spectrum acquired. The spectra were zapped at the 1646–1652 cm^{-1} range to remove the artifact caused by the chip-to-chip transition of the instrument. The spectra resolution is 2 cm^{-1}/pt. The spectra were processed using the programming language MATLAB and applied a Savitzky–Golay 0 polynomial order smoothing and area normalized. Processed data for each sample were split into three averaged spectra, 10 spectra averaged into 1, and applied a baseline correction (level + zero) and conducted peak fitting using GRAMS/AI Suite ThermoCorp software. Statistical analysis of peak fitting values for significance was analyzed using in-lab MATLAB script, running a set of t-tests, Anderson–Darling test, and Kruskal–Wallis test. One-way ANOVA followed by Tukey's HSD test was used to determine statistical significance of the data (Table 1).

2.2.5 | Circular Dichroism (CD)

The protein samples were initially diluted to a final concentration of 30 μM using phosphate-buffered saline (PBS) before analysis. CD spectra were then immediately recorded using a Jasco J-1000 CD spectrometer (Jasco, Easton, MD, USA). For each sample, three separate spectra were collected over the wavelength range 190–250 nm. These spectra were subsequently averaged to produce a single representative spectrum for each sample. The CD measurements were performed under identical conditions to ensure consistency and reliability of the data.

2.2.6 | Fourier-Transformed IR Spectroscopy (FTIR)

Protein samples were placed onto ATR crystal and dried at room temperature. Spectra were measured with 4 cm^{-1} resolution using Spectrum 100 FTIR spectrometer (Perkin-Elmer, Waltham, MA, USA). Three spectra were collected from each sample.

2.2.7 | Cell Toxicity Assays

Rat midbrain N27 cells (SCC048, Sigma-Aldrich, USA) were grown in RPMI-1640 Medium (Roswell Park Memorial Institute) (Thermo Fisher Scientific, Waltham, MA, USA) with 10% fetal bovine serum (FBS) (Invitrogen, Waltham, MA, USA) and antibiotic Normocin (InvivoGen, USA) in flat-base 96-well plate for challenging adherent cell type (83.3924.300, Sarstedt, Germany) (50 000 cells per well) at 37°C under 5% CO_2. The N27 cell line is not listed as a commonly misidentified cell line by the International Cell Line Authentication Committee (ICLAC; https://urldefense.com/v3/__http://iclac.org/databases/cross-contaminations/__;!!KwNVnqRv!A6feNIFR3Z6opHP87nGDWmopPhaTbEX_VwUWjsqVABVsZCUlePiS0vorZoZrPS8CMWRJCRb9Xfgg-4AZgcqqbn9Nl3byAg$). The cell line was not further authenticated. After 24 h, N27 cells were found to fully adhere to the bottom of wells. Cell confluency was ~70%–80%. Next, using a multichannel pipette, 100 μL of the cell culture was replaced with 100-μL RPMI-1640 Medium with 5% FBS. This cell media also had protein samples. After 24 h of incubation, we performed lactate dehydrogenase (LDH) assay using G1781 kit (Promega, Madison, WI, USA). Absorption readings were made in the plate reader (Tecan, Mannedorf, Switzerland) at 450 nm. Each well of the plate was measured at 25 points over the entire area of the well. One-way ANOVA followed by Tukey's HSD test was used to determine statistical significance of the data (Table 1). Cells used in the study had maximum of 10 passages.

2.2.8 | JC-1 Assay

Cell culture N27 (SCC048, Sigma-Aldrich, USA) was grown in RPMI-1640 Medium with 10% FBS and antibiotic Normocin (InvivoGen, USA). The cells were seeded in the amount of 50 000 cells per well in flat base 96-well plate (83.3924.300, Sarstedt, Germany) and incubated for 24 h at 37°C under 5% CO_2. The next day, we added samples and incubated for another 24 h at 37°C under 5% CO_2. The cells were removed, centrifuged at 400 g for 5 min, and resuspended in 100 μL of PBS. The cells were stained with MitoProbe JC-1 Assay Kit at a concentration of 2.0 μg/mL (M34152A, Thermo Fisher Scientific, USA). The cells are incubated in a CO_2 incubator for 30 min at 37°C. The cells were centrifuged at 400 g for 5 min and resuspended in 100 μL. The cells were detected using a flow cytometer (BD LSR II, Becton Dickinson, USA) using the red and green channels.

2.2.9 | Membrane Leakage Assay

Plasmids that code Chmp1b (cell membrane repair) and TFEB (lysosome biogenesis) were delivered in N27 rat dopaminergic neuronal cells using GeneX Plus Reagent (ACS-4004, ATCC, Manassas, VA, USA). N27 rat dopaminergic neuronal cells were grown in RPMI-1640 Medium (Roswell Park Memorial Institute) (Thermo Fisher Scientific, Waltham, MA, USA) with 10% FBS (Invitrogen, Waltham, MA, USA) in 96-well glass bottom plate with high performance (P96-1.5H-N, Cellvis, USA) (5,000 cells per well) at 37°C under 5% CO_2 until ~70%–80% confluency was reached. Cell transfection was performed in Dulbecco's modified Eagle medium (DMEM) (Thermo Fisher Scientific, Waltham, MA, USA) that contained no FBS for 4 h. After that, cell media were replaced on DMEM with 10% FBS and incubated for 24 h at 37°C in a 5% CO_2. Next, amyloid aggregates were added to N27 rat dopaminergic neuronal cells and incubated for 24 h at 37°C in a 5% CO_2. Imaging was performed using fluorescence microscope (EVOS M5000, Thermo Fisher Scientific, Waltham, MA, USA). Chmp1b and TFEB plasmids contain green fluorescence protein (GFP) (Figures S3 and S4). Microscopic images reported in Figures S3 and S4.show cells with various numbers of punctata present in each cell. Using these images, we counted the number of punctata in cells treated with Tau aggregates grown in the presence and absence of lipids. One-way ANOVA followed by Tukey's HSD test was used to determine statistical significance of the data (Table 1).

2.2.10 | Gene Expression

RNA was first extracted from N27 rat dopaminergic cells exposed to amyloids for 24 h using GeneJET RNA Purification Kit (Catalog No. K0732, Thermo Scientific). The concentration of extracted RNA was determined using a NanoDrop One Instrument (Thermo Scientific). cDNA synthesis was performed using SuperScript III Reverse Transcriptase (Catalog No. 18080093, Invitrogen) with random primers (Catalog No. 48190011, Invitrogen). Specific primers were designed for each target gene (Table S1) (Zhaliazka, Ali, and Kurouski 2024). qPCR was performed on C1000 Touch Thermal Cycler (BioRad) for 35–40 cycles. Each reaction mixture contained a cDNA, primers, and SYBR Green PCR master mix (Catalog No. 4309155, Applied Biosystems). β-Actin was used as a housekeeping gene to normalize the expression levels of the target genes. Nontemplate controls and positive controls were included in each qPCR run to ensure the accuracy and reliability of the results.

2.2.11 | Data Analysis

Statistical significance of reported results was analyzed using one-way ANOVA followed by Tukey's HSD test (Table 1). Prior to this, assessment of data normality was performed using Kolmogorov–Smirnov test. No tests for outliers were conducted on the data. The quantification of relative gene expression was determined using the comparative C_t method ($2^{-\Delta\Delta C_t}$), where ΔC_t represents the difference in threshold cycles between the target gene and the housekeeping gene and $\Delta\Delta C_t$ represents the difference in ΔC_t values between the treated samples and the control samples. The relative gene expression levels were calculated and presented as fold changes compared with the control samples.

3 | Results

3.1 | Kinetic Studies of 0N4R, 1N4R, and 2N4R Tau Aggregation in the Presence of LUVs With Low, Physiological, and Elevated Concentrations of Cholesterol

Using a ThT assay, we examined the extent to which the concentration of cholesterol in membranes could alter the rate of 0N4R, 1N4R, and 2N4R Tau aggregation. For this, proteins were mixed at equimolar concentrations with LUVs that contained 10:90 (Cho:PC(10:90)) and 45:55 (Cho:PC(45:55)) ratios of cholesterol and DMPC, which resembles low and physiological concentrations of Cho in the plasma membranes of neurons. The same experiments were performed with LUVs that contained 60:40 ratio of Cho and DMPC (Cho:PC(60:40)), which resembled lipid membranes with high concentrations of cholesterol, as well as LUVs composed of 100% DMPC (PC) (control). Finally, we performed the aggregation of 0N4R, 1N4R, and 2N4R Tau in the lipid-free environment.

At pH 7.4, 0N4R Tau aggregated with a well-defined lag-phase (t_{lag}) of 66.53 ± 1.40 h (Figure 1). The lag phase was followed by a rapid increase in ThT fluorescence, which indicated the formation of amyloid fibrils. We also found that in the presence of Cho:PC (10:90) and PC, no increase in ThT intensity was observed during 350 h. These results indicated that LUVs with low concentrations of cholesterol, as well as zwitterionic membranes, strongly inhibited 0N4R Tau aggregation. At the same time, an increase in the concentration of cholesterol to 45% and 60% resulted in 0N4R Tau aggregation lag phase (t_{lag}) of 254.53 ± 20.71 h and 202.23 ± 35.25, respectively. However, a substantial delay in both t_{lag} and $t_{1/2}$ was observed. These results indicated that physiological and elevated concentrations of cholesterol delayed the aggregation of 0N4R Tau.

Similar results were observed for 1N4R Tau isoform. Specifically, we found no changes in the ThT signal during 350 h for 1N4R Tau aggregated in the presence of LUVs composed of Cho:PC (10:90) and PC, whereas in the lipid-free environment, 1N4R Tau aggregated with t_{lag} of 30.64 ± 3.08 (Figure 1). Similar to 0N4R Tau, Cho:PC (45:55) strongly delayed both t_{lag} and $t_{1/2}$ (255.24 ± 22.69 h and 336.45 ± 18.779, respectively). The same effect was observed for Cho:PC (60:40) for both t_{lag} and $t_{1/2}$ (123.20 ± 8.96 and 197.49 ± 12.36, respectively). However, substantially weaker deceleration of 0N4R Tau aggregation was observed compared to Cho:PC (45:55). These results indicated that physiological concentrations of cholesterol strongly disfavored 1N4R Tau aggregation, whereas this effect was less evident for lipid vesicles with high concentrations of cholesterol. Similar to 0N4R Tau, LUVs with low concentrations of cholesterol, as well as zwitterionic membranes, strongly inhibited the aggregation of 1N4R Tau isoform.

Kinetic studies of 2N4R Tau in the presence of LUVs with different concentrations of cholesterol revealed drastically different protein behavior compared to 0N4R and 1N4R Tau isoforms discussed above. We observed no changes in ThT signal in all samples except Cho:PC (60:40), which delayed 2N4R Tau aggregation (t_{lag} = 81.47 ± 13.2 h) compared to the lipid-free

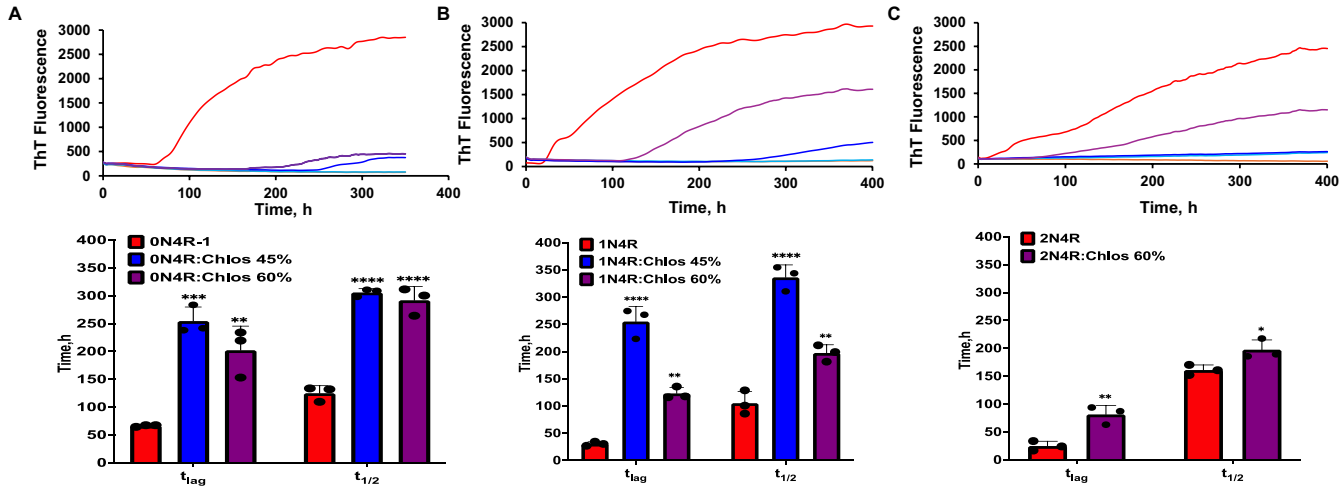

FIGURE 1 | Cholesterol alters the rate of Tau aggregation. ThT kinetics (top row) and corresponding histograms (bottom row) of t_{lag} and $t_{1/2}$ for 0N4R (A), 1N4R (B), and 2N4R (C) aggregation in the lipid-free environment (red), as well as in the presence of 10:90 Cho:PC (light blue), 45:55 Cho:PC (blue), 60:40 Cho:PC (purple), and PC (orange). Each curve shown in panels A–C is the average of three independent replicates ($n = 3$). The graphical data are presented as the mean ± SEM. According to one-way ANOVA followed by Tukey's HSD test, $^{*}p < 0.05$, $^{**}p < 0.01$, $^{***}p < 0.001$, and $^{****}p < 0.0001$.

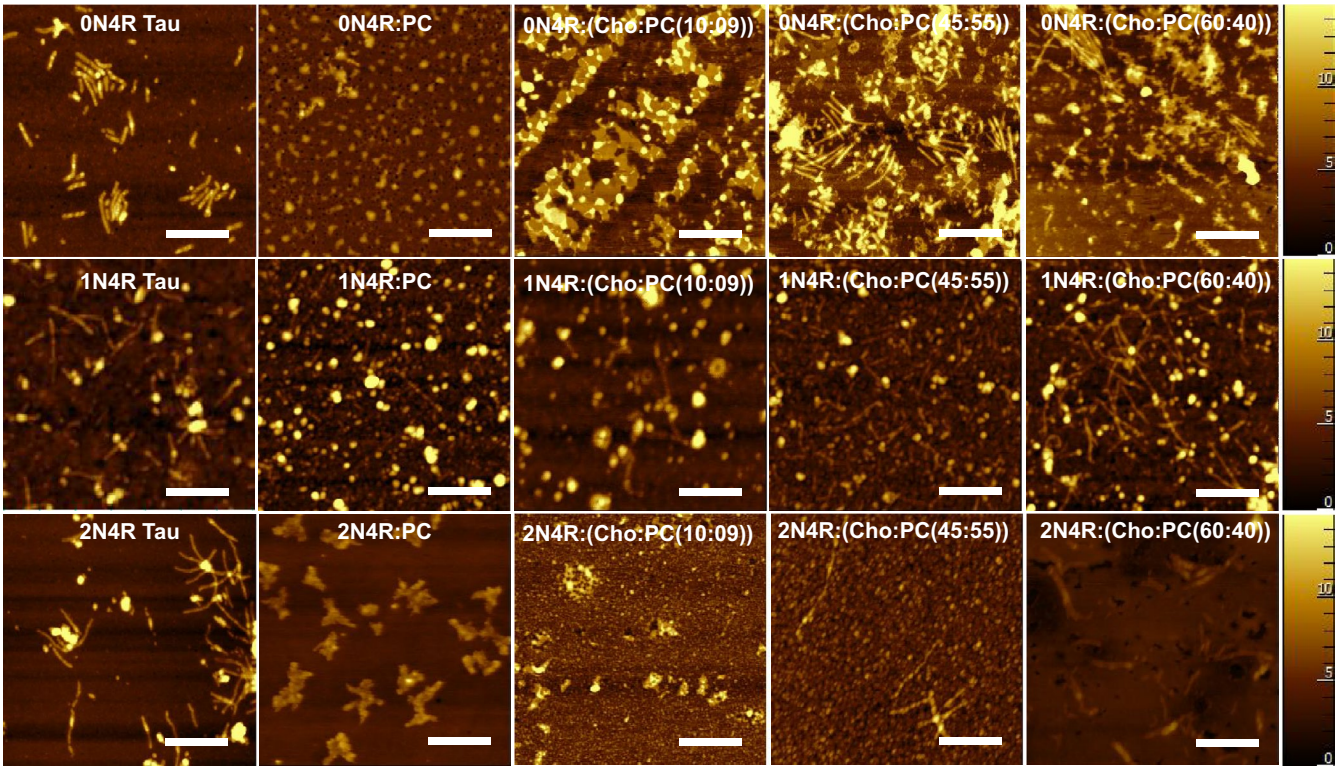

FIGURE 2 | Cholesterol changes morphology of protein aggregates. AFM images of amyloid aggregates formed by different Tau isoforms in the lipid-free environment (0N4R, 1N4R, and 2N4R), as well as in the presence of PC, 10:90 Cho:PC, 45:55 Cho:PC, and 60:40 Cho:PC.

environment ($t_{lag} = 22.27 \pm 7.50$) (Figure 1). Based on these results, we could conclude that 2N4R Tau isoform aggregated only at the high concentrations of cholesterol in the lipid membranes. These results also indicated that the presence of two N-terminal repeat prevented the self-assembly of 2N4R Tau into toxic amyloid fibrils at low and physiological concentrations of cholesterol in plasma membranes.

3.2 | Morphological Characterization of 0N4R, 1N4R, and 2N4R Tau Aggregates Grown in the Presence of LUVs With Low, Physiological, and Elevated Concentrations of Cholesterol

Atomic force microscopy revealed that in the lipid-free environment, 0N4R Tau formed short fibrils that were ~ 5–6 nm

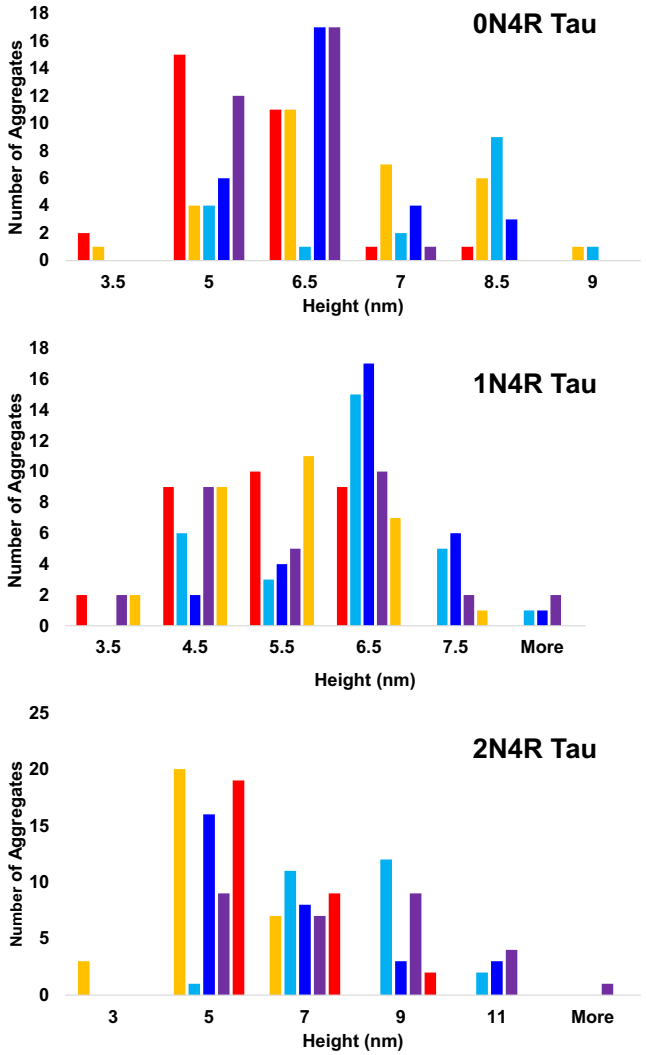

FIGURE 3 | Cholesterol changes the height of protein aggregates. Histograms of height distribution of amyloid aggregates formed by different Tau isoforms in the lipid-free environment (red), as well as in the presence of 10:90 Cho:PC (light blue), 45:55 Cho:PC (blue), 60:40 Cho:PC (purple), and PC (orange).

in height (Figures 2 and 3). We also observed some oligomers co-present together with fibrils. AFM showed that PC and 10:90 Cho:PC fully inhibited fibril formation. In 0N4R:PC, we observed only spherical oligomers that were 5–8 nm in diameter. Morphologically similar aggregates were observed in 0N4R:Cho:PC(10:90). However, these aggregates were substantially larger (7–9 nm) compared to amyloid oligomers that were present in 0N4R:PC and 0N4R Tau samples (Figures 2 and 3). These results indicated that PC and low concentrations of cholesterol fully inhibited 0N4R Tau fibrillization. At the same time, in the presence of LUV composed of 45:55 Cho:PC, we observed the presence of thick fibrils that were 5–8 nm in height. These protein aggregates were morphologically similar to those formed by 0N4R Tau in the lipid-free environment. Morphologically similar, however, slightly thinner fibrils were also observed in 0N4R:Cho:PC(60:40). These results indicated that LUVs with physiological and elevated concentrations of cholesterol did not significantly change the morphology of protein aggregates compared to those formed in the lipid-free environment.

We also found that in the lipid-free environment, 1N4R Tau formed thin fibrils with a height ranging from 4 to 7 nm. However, these fibrillar species were less abundant in 1N4R:PC that was dominated by very short elongated species and spherical oligomers that were 4–7 nm in height (Figures 2 and 3). 1N4R:Cho:PC(10:90) possessed thin filaments that also were 4–7 nm in height. We found that such filaments were far more abundant in 1N4R:Cho:PC(45:55) and 1N4R:Cho:PC(60:40). Their height ranged from 5 to 10 nm. These results indicated that LUVs composed of PC and low concentration of cholesterol strongly disfavored fibrillization of 1N4R Tau isoform. However, at physiological and elevated concentrations of cholesterol, 1N4R Tau formed amyloid aggregates similar to 0N4R Tau isoform. In the lipid-free environment, 2N4R Tau formed thin fibrils that were 5–9 nm in height. We also found that PC and Cho:PC(10:90) fully inhibited 2N4R Tau aggregation.

In the presence of LUVs with PC and low concentration of cholesterol (Cho:PC(10:90)), we observed only small oligomers 3–7 and 5–9 nm, respectively. AFM revealed that 2N4R:Cho:PC(45:55) was largely dominated by thin oligomers that were 5–11 nm in height. We also observed a small amount of filaments that were ~8 nm in height (Figures 2 and 3). Such filaments were highly abundant in 2N4R:PC and Cho:PC(60:40) samples. Their height ranged from 5 to 11 nm. Based on these results, we could conclude that LUVs with low concentrations of cholesterol strongly suppressed the fibrillization of both 1N4R and 2N4R Tau. However, the presence of LUVs with high concentrations of cholesterol resulted in the formation of morphologically similar aggregates formed by these Tau isoforms in the lipid-free environment.

3.3 | Structural Characterization of 0N4R, 1N4R, and 2N4R Tau Aggregates Grown in the Presence of LUVs With Low, Physiological, and Elevated Concentrations of Cholesterol

FTIR was used to examine the secondary structure of 0N4R Tau aggregates formed in the presence of LUVs with low, physiological, and elevated concentrations of cholesterol. Acquired FTIR spectra exhibited amide I (1620–1700 cm^{-1}), amide II (1520–1580 cm^{-1}), and Cα-H (~1460 cm^{-1}) bands (Kurouski 2023). In all acquired spectra, amide I band was centered around 1645 cm^{-1}, which indicated the dominance of α-helical protein in the analyzed samples (Figure 4) (Ali et al. 2023c, 2023d). We also found that samples that contained 1N4R and 2N4R Tau aggregates grown in the presence of LUVs with low, physiological, and elevated concentrations of cholesterol exhibited amide I band centered around 1630 cm^{-1}, which indicated the predominance of parallel β-sheet in the secondary structure of amyloid fibrils present in these samples. This conclusion was further supported by CD. We found that CD spectra acquired from all samples had a minimum at ~225 nm, which corresponded to β-sheet secondary structure (Figure 4).

In the spectra acquired from 1N4R:PC and Cho:PC (60:40) samples, amide I band was blue shifted to 1621 cm^{-1}, which may suggest structural differences between 1N4R:PC and Cho:PC (60:40) fibrils and fibrils formed in the presence of LUVs with low and medium concentrations of cholesterol (Figure 4). Similar shifts in

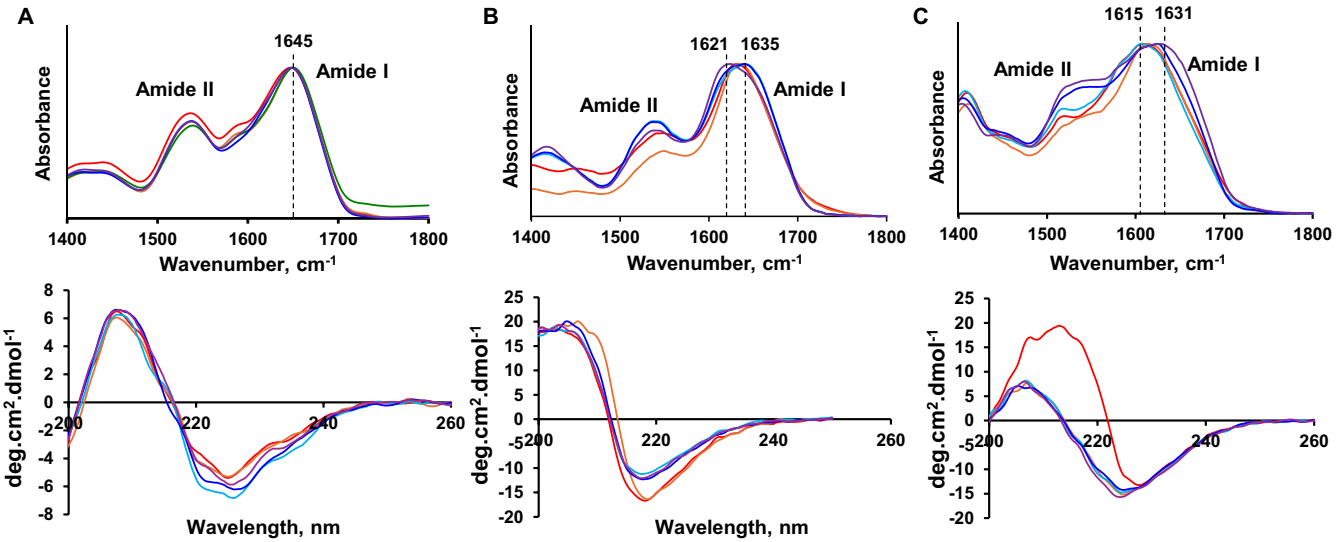

FIGURE 4 | Secondary structure of protein aggregates. FTIR (top panels) and CD (bottom panels) spectra acquired from amyloid aggregates formed by 0N4R (A), 1N4R (B), and 2N4R (C) in the lipid-free environment (red), as well as in the presence of 10:90 Cho:PC (light blue), 45:55 Cho:PC (blue), 60:40 Cho:PC (purple), and PC (orange). Each curve shown in Panels A–C is the average of three sample replicates ($n = 3$).

the position of amide I band were observed in 2N4R Tau aggregates formed in the presence of LUVs with low, physiological, and elevated concentrations of cholesterol. These results indicated that differences in the concentrations of cholesterol in LUVs could result in differences in the secondary structure of 1N4R and 2N4R Tau fibrils that were formed in their presence. We also found that CD spectra of 1N4R Tau fibrils that were formed in the presence of LUVs with 10:90 Cho:PC and PC had slightly blue-shifted minima compared to CD spectra of 1N4R Tau fibrils formed in the presence of LUVs with Cho:PC (45:55) and Cho:PC (60:40). This observation further supports the discussed above possible differences in the secondary structure of protein aggregates. At the same time, both FTIR and CD probe, the secondary structure of bulk volume of the samples, also contain unaggregated protein. One can expect that signal from the monomeric protein could cause the abovementioned spectral variability.

To overcome this problem and to elucidate the secondary structure of protein aggregates present in each sample, we employed AFM-IR spectroscopy (Figure 5). AFM-IR allows for acquisition of IR spectra from individual oligomers and fibrils via positioning of the scanning probe on their surfaces. Using AFM-IR, we found that the secondary structure of all Tau aggregates was dominated by parallel β-sheet with a small amount of unordered protein and antiparallel β-sheet (Figure 5). We also found that the presence of LUVs at the stage of protein aggregation did not cause substantial changes in the secondary structure of oligomers and fibrils formed by 0N4R, 1N4R, and 2N4R Tau isoforms (Figure 5). We also found that 0N4R:PC aggregates possessed slightly lower amounts of antiparallel β-sheet compared to 0N4R Tau fibrils grown in the lipid-free environment. Based on these results, we can conclude that the presence of LUVs does not alter the secondary structure of 0N4R, 1N4R, and 2N4R Tau fibrils.

3.4 | Toxicity of 0N4R, 1N4R, and 2N4R Tau Aggregates Grown in the Presence of LUVs With Low, Physiological, and Elevated Concentrations of Cholesterol

We used LDH assay to examine the cytotoxicity of 0N4R, 1N4R, and 2N4R Tau aggregates formed in the presence of LUVs with different concentrations of cholesterol. We found that low and physiological concentrations of cholesterol enhanced cytotoxicity of 0N4R Tau fibrils (Figure 6). The same conclusion could be made about LUVs composed of only PC. However, we found no significant changes in the toxicity of 0N4R Tau fibrils formed in the lipid-free environment and the presence of Cho:PC(60:40). At the same time, low, physiological, and elevated concentrations of cholesterol strongly increased cytotoxicity of 1N4R Tau fibrils. We also found that LUVs composed of only PC slightly lowered the toxicity of 1N4R Tau fibrils compared to 1N4R Tau aggregates formed in the lipid-free environment (Figure 6). Interestingly, the presence of cholesterol did not increase the cytotoxicity of 2N4R Tau fibrils. Furthermore, we observed a small decrease in the cytotoxicity of 2N4R:(Cho:PC(10:90)) and 2N4R:(Cho:PC(60:40)) fibrils compared to 2N4R Tau aggregates formed in the lipid-free environment (Figure 6). Cytotoxicity of 2N4R:PC and 2N4R:(Cho:PC(45:55)) fibrils was the same as the toxicity of 2N4R Tau fibrils grown in the absence of LUVs. It should be noted that LUVs themselves exerted no cytotoxic effects on N27 rat dopaminergic cells (Figure 6). Based on these results, we can conclude that the presence of 2 N repeat in Tau prevents a cholesterol-induced increase in cytotoxicity of amyloid aggregates. At the same time, Tau isoforms without this insert aggregate forming, on average, more toxic aggregates in the presence of lipids compared to the lipid-free environment.

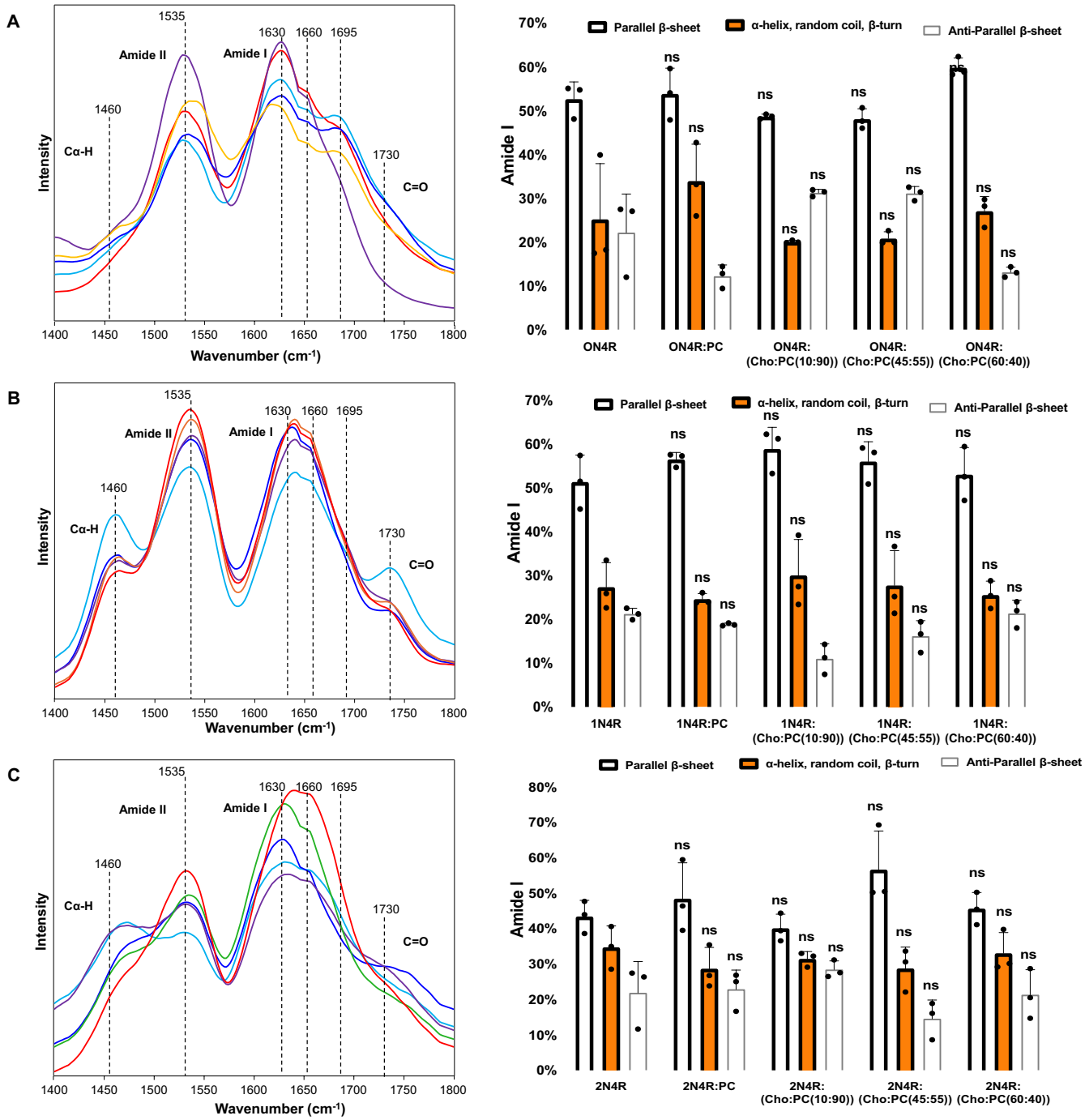

FIGURE 5 | AFM-IR spectra (left) and histograms (right) showing the amount of parallel β-sheet (blue), α-helix, random coil, and β-turn (orange), as well as antiparallel β-sheet (gray) in the secondary structure of 0N4R (A), 1N4R (B), and 2N4R (C) Tau aggregates grown in the lipid-free environment (red), as well as in the presence of 10:90 Cho:PC (light blue), 45:55 Cho:PC (blue), 60:40 Cho:PC (purple), and PC (orange). Each curve shown in panels A–C is the average of three sample replicates ($n = 3$). The graphical data are presented as the mean ± SEM. According to one-way ANOVA followed by Tukey's HSD test, $^{*}p < 0.05$, $^{**}p < 0.01$, $^{***}p < 0.001$, and $^{****}p < 0.0001$. NS shows the absence of statistically significant differences.

3.5 | Elucidation of Molecular Mechanisms of Toxicity of 0N4R, 1N4R, and 2N4R Tau Aggregates Grown in the Presence of LUVs With Low, Physiological, and Elevated Concentrations of Cholesterol

Amyloid aggregates enter the cell primarily via endocytosis (Matveyenka et al. 2023; Matveyenka, Zhaliazka, and Kurouski 2024). This results in their localization in cell endosomes (Matveyenka et al. 2023; Matveyenka, Zhaliazka, and Kurouski 2024). Previously reported results by our groups showed that uptake of α-syn, $A\beta_{1\text{-}42}$, and insulin fibrils by neurons caused damage of cell endosomes with the following impairment of cell mitochondria and endoplasmic reticulum (ER). As a result of endosomal damage, cells upregulate genes responsible for endosomal repair, de novo biogenesis of organelles, and clearance of damaged endosomes by autophagy (Kondow-McConaghy et al. 2020). Expanding upon this, we used a set

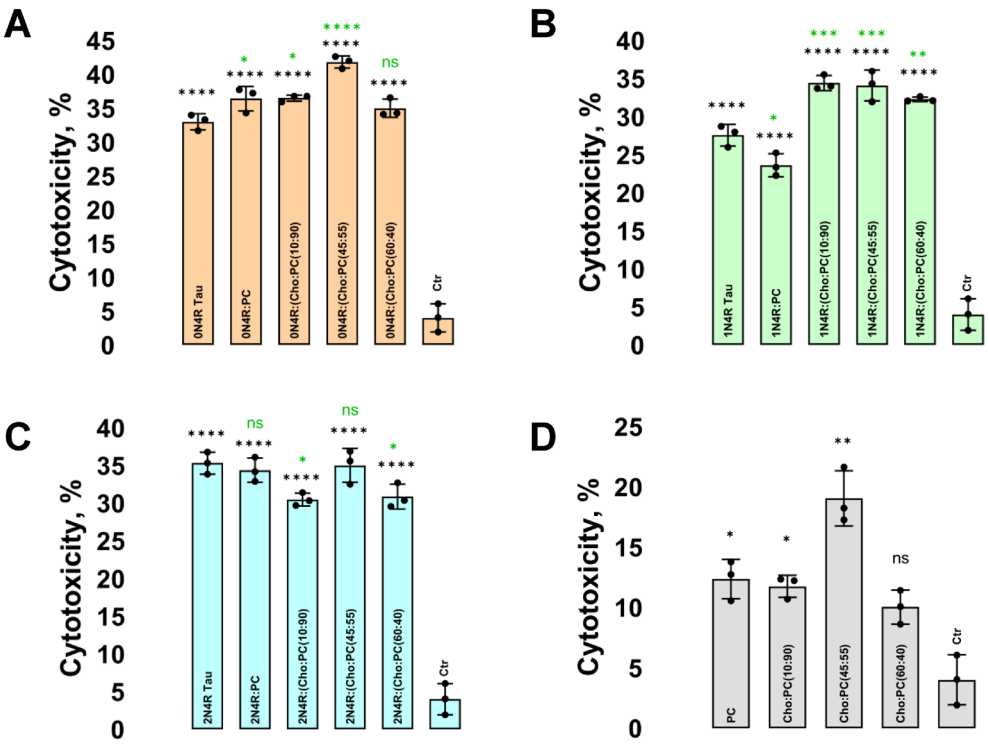

FIGURE 6 | Cholesterol alters toxicity of Tau fibrils. Histograms of LDH assay revealing cytotoxicity of 0N4R (A), 1N4R (B), and 2N4R (C) Tau fibrils grown in the lipid-free environment and the presence of LUVs composed of 10:90 Cho:PC, 45:55 Cho:PC, 60:40 Cho:PC, and PC, as well as lipids themselves (D). Each curve shown in Panels A–C is the average of three biological replicates ($n = 3$); each well contained 50 000 cells. The graphical data are presented as the mean ± SEM. According to one-way ANOVA followed by Tukey's HSD test, black asterisk (*) shows differences in the cytotoxicity between samples and control (ctr), whereas green asterisk shows differences in the cytotoxicity among 0N4R, 1N4R, and 2N4R grown in the lipid-free environment and the presence of LUVs; *$p < 0.05$, **$p < 0.01$, ***$p < 0.001$, and ****$p < 0.0001$. NS—nonsignificant difference.

of molecular markers to investigate the extent to which 0N4R, 1N4R, and 2N4R Tau aggregates grown in the presence of LUVs with low, physiological, and elevated concentrations of cholesterol caused endosomal damage in N27 rat dopaminergic neurons.

The magnitude of endosomal damage can be determined by elucidation of changes in the expression of Chmp1, a marker protein that binds to damaged endosomal membranes to activate ESCRT-III complex involved in the membrane repair (Kondow-McConaghy et al. 2020; Skowyra et al. 2018; Radulovic et al. 2018). Therefore, in our experiments, N27 rat dopaminergic neurons were transfected with Chmp1-EGFP construct and exposed to 0N4R, 1N4R, and 2N4R Tau aggregates grown in the presence of LUVs with low, physiological, and elevated concentrations of cholesterol. Next, we utilized fluorescence microscopy to quantify the localization of the expression products of Chmp1-EGFP and, consequently, the extent to which Tau aggregates damage cell endosomes. In healthy cells, Chmp1 has a diffuse spread across the cytosol, while in the cells with damaged endosomes, Chmp1 forms puncta-like inclusions (Figures S3 and S4). Consequently, the greater the number of punctata in the cell, the larger the magnitude of the endosomal damage. We found that 0N4R, 1N4R, and 2N4R Tau aggregates formed in the presence of low, physiological, and high concentrations of cholesterol-damaged cell endosomes, which resulted in the activation of ESCRT-III complex and the membrane repair (Figure 7). However, this effect was not observed for 0N4R, 1N4R, and 2N4R Tau aggregates grown in the presence of PC. We also found that 1N4R Tau, 1N4R:Cho:PC(45:55), and 1N4R:Cho:PC(60:40) triggered the greatest magnitude of membrane repair in neurons, and consequently, endosomal damage compared to other protein aggregates.

Endosomal Ca^{2+} efflux caused by endosomal damage also activates TFEB, a transcription factor that regulates lysosomal biogenesis and autophagy (Settembre et al. 2011; Sardiello et al. 2009; Medina et al. 2015). Activated TFEB is transported to the nucleus where it activates a transcriptional program that induces de novo biogenesis of endosomal organelles (Kondow-McConaghy et al. 2020). Therefore, we transfected N27 rat dopaminergic neurons with TFEB-EGFP to determine the extent to which Tau aggregates induced de novo biogenesis of endosomes (Figures S3 and S4). We found that all 0N4R, 1N4R, and 2N4R Tau aggregates triggered intense de novo biogenesis of endosomal organelles. These findings indicate that endocytosis of Tau aggregates caused severe endosomal damage. We also found that 2N4R Tau and 2N4R aggregates formed in the presence of Cho:PC(45:55) and Cho:PC(60:40) triggered the greatest magnitude of de novo biogenesis in the cells (Figure 7).

One can expect that leakage of protein aggregate into the cell cytosol could cause strong damage to cell organelles including ER and mitochondria. Therefore, we used qPCR to investigate whether exposition of N27 rat dopaminergic neurons to Tau aggregates would cause changes in the expression of proteins responsible for unfolded protein response (UPR) of cell ER. UPR activates a set of signaling pathways in cells that aim to

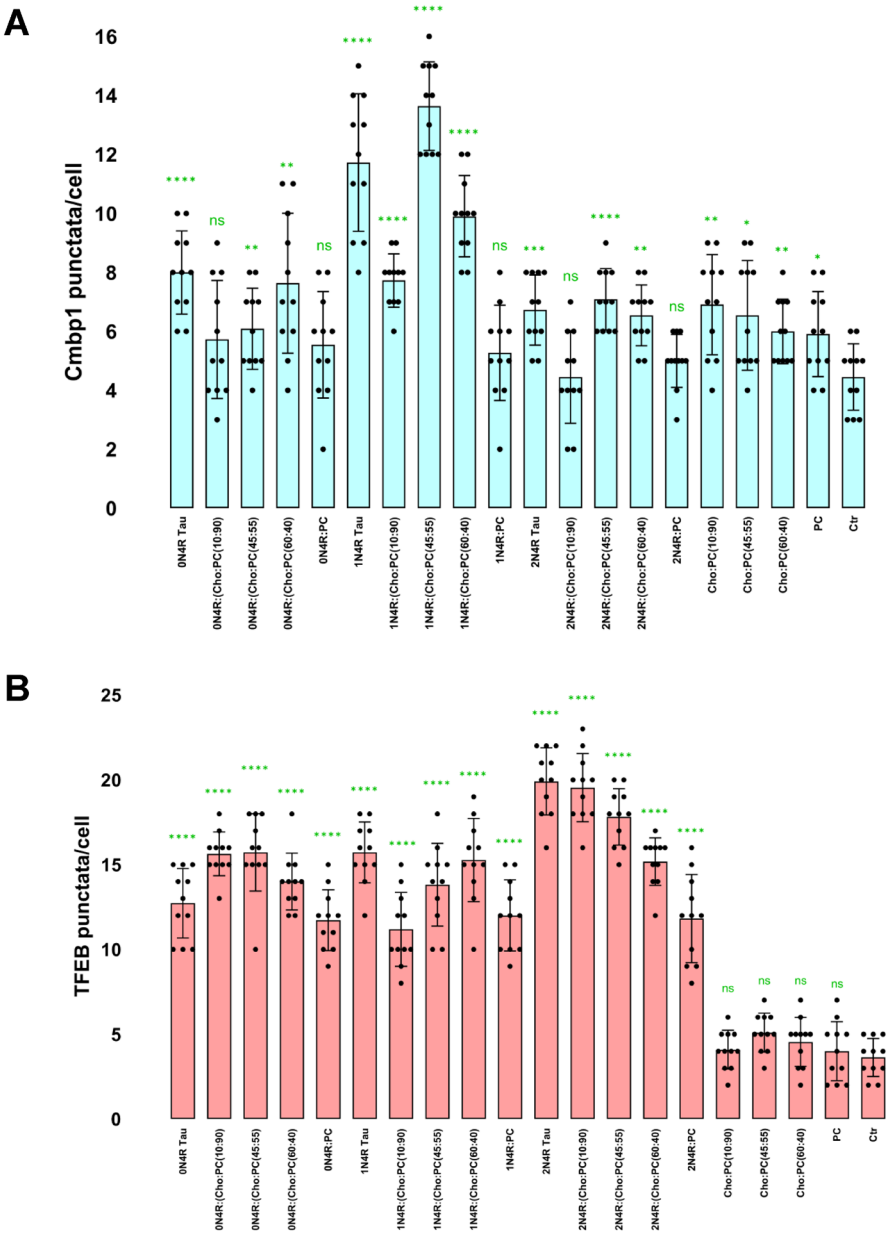

FIGURE 7 | Molecular mechanism of amyloid toxicity. Histograms of fluorescent puncta per cell observed in N27 rat dopaminergic cells after their incubation with 0N4R, 1N4R, and 2N4R Tau fibrils grown in the lipid-free environment and in the presence of LUVs composed of 10:90 Cho:PC, 45:55 Cho:PC, 60:40 Cho:PC, and PC, as well as lipids themselves. For each of the presented results, at least 15 individual images were analyzed. Each curve shown in Panels A–B is the average of three biological replicates ($n = 3$); each well contained 50000 cells. The graphical data are presented as the mean ± SEM. According to one-way ANOVA followed by Tukey's HSD test, $^{*}p < 0.05$, $^{**}p < 0.01$, $^{***}p < 0.001$, and $^{****}p < 0.0001$. NS, nonsignificant difference.

mitigate ER stress and restore cell homeostasis (Oslowski and Urano 2011). The UPR is induced by transmembrane proteins PKR-like ER kinase (PERK) and activating transcription factor 6 (ATF6) (Urano, Bertolotti, and Ron 2000; Calfon et al. 2002; Shen et al. 2001). These proteins are regulated by BiP, a 78-kDa glucose-regulated chaperon GRP78 (Adams et al. 2019; Kopp et al. 2019). Under ER stress, GRP78 dissociates from PERK and ATF6 causing their activation (Bertolotti et al. 2000; Harding et al. 2000). In addition to PERK and ATF6, UPR activates inositol requiring 1 (IRE1) kinase senses unfolded or misfolded proteins by its N-terminal luminal domain (Harding, Zhang, and Ron 1999). Activated IRE1 autophosphorylates splicing of X-box binding protein 1 (XBP-1), which migrates in the nucleus where it upregulates UPR target genes, as well as genes that encode folding proteins such as protein disulfide isomerase and chaperones (Lee, Iwakoshi, and Glimcher 2003; Iwakoshi, Lee, and Glimcher 2003; Lee et al. 2003).

We found that 0N4R, 1N4R, and 2N4R Tau aggregates grown in the presence of LUVs with low, physiological, and elevated concentrations of cholesterol caused strong upregulation of PERK, ATF6, and XBP1 (Figure 8 and Figure S5). We also found that activation of UPR signaling pathways is linked to the structure of the protein aggregates. For instance, 2N4R Tau aggregates formed in the absence of lipids, primarily activated XBP1 UPR signaling pathway, whereas corresponding Tau aggregates that

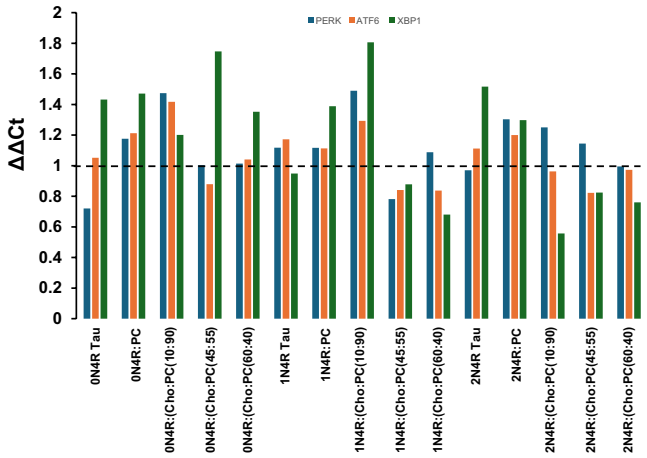

FIGURE 8 | Cholesterol alters the extent to which Tau aggregates cause UPR in ER of N27 rat dopaminergic neurons. Histograms of relative expression of PERK, ATF6, and XBP1 in N27 rat dopaminergic neurons after cell exposition of 0N4R, 1N4R, and 2N4R Tau fibrils grown in the lipid-free environment and in the presence of LUVs composed of 10:90 Cho:PC, 45:55 Cho:PC, 60:40 Cho:PC, and PC. Each curve shown in Panels A–C is the average of three biological replicates ($n = 3$); each well contained 50 000 cells.

were grown in the presence of lipids caused a strong activation of PERK kinase. Based on these results, we can conclude that 0N4R, 1N4R, and 2N4R Tau aggregates grown in the presence of LUVs with low, physiological, and elevated concentrations of cholesterol exert cytotoxicity by causing a strong impairment of ER in neuronal cells.

Next, we used JC1 assay to examine the extent to which 0N4R, 1N4R, and 2N4R Tau aggregates formed in the presence of LUVs with different concentrations of cholesterol damage cell mitochondria. Our results show that amyloid fibrils formed by all isoforms caused severe mitochondrial damage in N27 rat dopaminergic cells. We also found that 0N4R Tau aggregates grown under low and physiological concentrations of cholesterol exert the same magnitude of damage of cell mitochondria as 0N4R Tau aggregates formed in the lipid-free environment (Figure 9). However, the presence of LUVs with high concentrations of cholesterol caused a decrease in the mitochondrial cytotoxicity of 0N4R Tau fibrils. Our results also showed that the presence of lipids at the stage of 1N4R Tau aggregation lowers their mitochondrial cytotoxicity. Finally, we found that only LUVs with low and physiological concentrations of Cho increased the extent to which 2N4R Tau fibrils damage cell mitochondria, whereas LUVs composed of PC and Cho:PC(60:40) did not alter mitochondrial cytotoxicity of 2N4R Tau fibrils. Our results also showed that LUVs themselves cause only a very small increase in mitochondrial depolarization compared to the control. These results indicate that cholesterol uniquely alters cytotoxicity of Tau aggregates to the cell mitochondria.

4 | Discussion

All Tau isoforms are natively unfolded, intrinsically disordered, and soluble proteins that are abundantly expressed in the central and peripheral nervous system. The isoforms facilitate microtubular assembly in the cells binding with their N-terminal inserts to tubulin. Experimental findings recently reported by Ali et al. (2024) showed that N-terminal inserts in 2N4R Tau isoform also play an important role in protein–lipid interaction. Specifically, the rate of 2N4R Tau aggregation could be uniquely altered by PS, whereas such changes in the rate of protein aggregation were not observed for 1N4R Tau isoform that lacks the second N-ter minal insert. Thus, the second N insert is highly important for protein stability. Our current findings show that Tau isoforms that lack this insert (0N4R and 1N4R Tau) become unstable and are prone to aggregate at the physiological concentration of cholesterol. However, 2N4R Tau remains stable for over 350 h in the presence of lipid vesicles that possess physiological concentrations of cholesterol. It should be noted that all analyzed Tau isoforms do not form fibrils in the presence of LUVs with low concentrations of cholesterol, which is in good agreement with the recently reported results by Mammeri and coworkers (El Mammeri et al. 2023). Experimental results reported by Hong group also indicate that this effect is linked to the size of the lipid vesicles. Specifically, the researchers demonstrated that unlike LUVs, small unilamellar vesicles (SUVs) facilitate aggregation of 0N4R Tau isoform into long fibrils that exhibit the characteristic β-sheet (El Mammeri et al. 2023).

We also found that low, physiological, and high concentrations of cholesterol in lipid membranes alter the morphology of 0N4R, 1N4R, and 2N4R Tau aggregates that were formed in their presence. However, we observed no change in the secondary structure of such aggregates compared to 0N4R, 1N4R, and 2N4R Tau fibrils formed in the lipid-free environment. These results suggest that lipids do not template Tau aggregation but rather alter the stability of monomeric proteins. It should be noted that such lipid-templated aggregation was previously reported for $A\beta_{1\text{-}42}$ (Zhaliazka, Matveyenka, and Kurouski 2023), α-syn (Dou and Kurouski 2022; Dou, Matveyenka, and Kurouski 2023), and TTR (Ali, Zhaliazka, Dou, Holman, Kumar et al. 2023; Ali et al. 2023a, 2023b). In these cases, proteins form structurally different aggregates in the presence of lipids compared to the fibrils observed in the lipid-free environment.

Our findings show that the presence of cholesterol in the lipid membranes causes a strong increase in the toxicity of 0N4R Tau and 1N4R Tau fibrils, whereas this effect of cholesterol was not observed for 2N4R Tau isoform. These findings indicate that the second N insert is the key element in the Tau sequence that lowers the cytotoxicity of Tau aggregates. Additional studies are required to fully understand molecular mechanisms of the observed N-insert–determined changes in the cytotoxicity of amyloid aggregates. Nevertheless, we demonstrated that Tau oligomers and fibrils that were formed in the presence of LUVs with low, physiological, and elevated concentrations of cholesterol damage cell endosomes and mitochondria, as well as cause severe impairment activating UPR of ER. Such impairments ultimately lead to the cell death. These results are consistent with experimental findings that were previously reported by Ali et al. (2024) for 1N4R and 2N4R Tau aggregates formed in the presence of PS with different lengths and saturations of fatty acids. Specifically, the researchers showed that Tau fibrils formed by both isoforms endocytosed by neuronal cells. As a

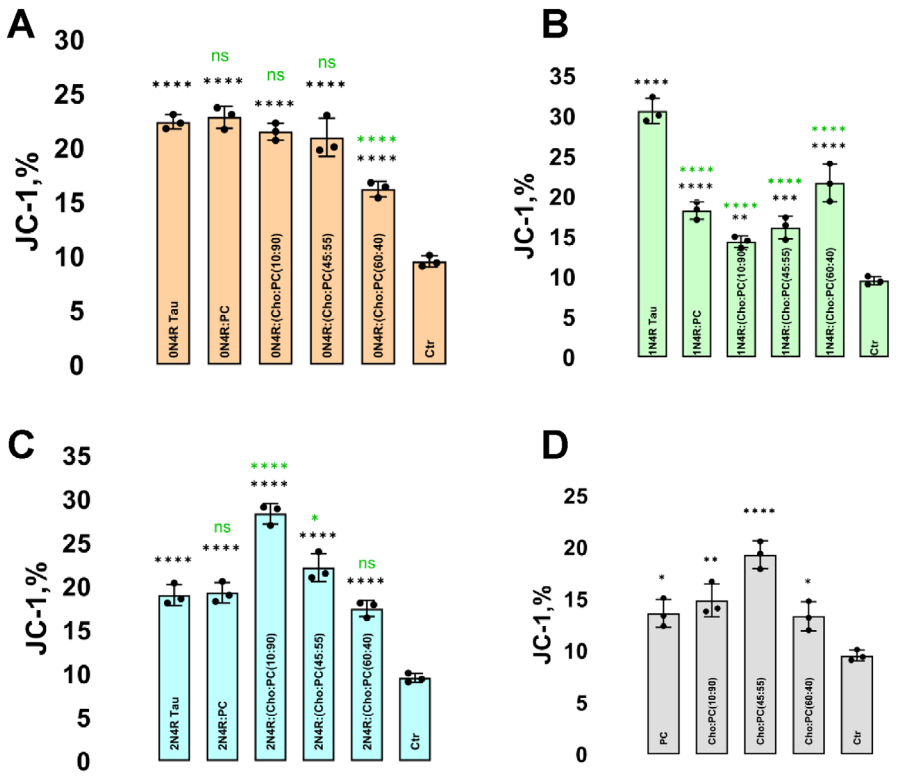

FIGURE 9 | Cholesterol alters the extent to which Tau aggregates damage mitochondria in N27 rat dopaminergic neurons. Histograms of JC-1 assay revealing mitochondria damage exerted by 0N4R (A), 1N4R (B), and 2N4R (C) fibrils grown in the lipid-free environment and the presence of LUVs composed of 10:90 Cho:PC, 45:55 Cho:PC, 60:40 Cho:PC, and PC, as well as lipids themselves (D). Each curve shown in Panels A–C is the average of three biological replicates ($n = 3$); each well contained 50 000 cells. The graphical data are presented as the mean ± SEM. According to one-way ANOVA followed by Tukey's HSD test, black asterisks (*) show differences in the cytotoxicity between samples and control (ctr), whereas green asterisks show differences in the cytotoxicity among 0N4R, 1N4R, and 2N4R grown in the lipid-free environment and the presence of LUVs; *$p < 0.05$, **$p < 0.01$, ***$p < 0.001$, and ****$p < 0.0001$. NS—nonsignificant difference.

result, these aggregates damage cell mitochondria and enhance ROS levels in cells. Similar to our findings, the researchers demonstrated that structurally and morphologically different aggregates activate the same molecular pathways of endosomal damage and mitochondrial UPR.

5 | Conclusions

Our results demonstrate that 0N4R, 1N4R, and 2N4R Tau isoforms can aggregate forming toxic amyloid oligomers and fibrils. We also found rates of their aggregation could be altered by cholesterol present in the lipid bilayer. At low concentrations of cholesterol, the aggregation of all three isoforms was strongly inhibited. Physiological concentrations of cholesterol only inhibit the aggregation of 2N4R Tau, whereas 0N4R and 1N4R Tau aggregate at the physiological concentrations of cholesterol forming highly toxic oligomers and fibrils. These results indicate that the second N-terminal insert plays an important role in protein–lipid interactions. We also found that elevated concentrations of cholesterol trigger the aggregation of all Tau isoforms. Biophysical methods utilized in our study did not reveal substantial structural differences between amyloid fibrils formed by Tau isoforms in the presence and absence of lipids. These results suggest that lipids only alter the stability of monomeric proteins rather than template their aggregation. Thus, aging-related increase in the concentration of cholesterol in plasma membranes could be linked to the onset of tauopathies and AD.

Author Contributions

Abid Ali: conceptualization, investigation, methodology, writing – review and editing, visualization, writing – original draft. **Mikhail Matveyenka:** writing – original draft, writing – review and editing, investigation, methodology. **Davis N. Pickett:** investigation, methodology, visualization, validation. **Axell Rodriguez:** investigation, methodology, visualization, validation. **Dmitry Kurouski:** conceptualization, funding acquisition, writing – original draft, writing – review and editing, project administration, supervision, resources.

Acknowledgments

We are grateful to the National Institute of Health for providing financial support (R35GM142869).

Conflicts of Interest

The authors declare no conflicts of interest.

Data Availability Statement

The data that support the findings of this study are available from the corresponding author upon reasonable request.

References

Adams, C. J., M. C. Kopp, N. Larburu, P. R. Nowak, and M. M. U. Ali. 2019. "Structure and Molecular Mechanism of ER Stress Signaling by the Unfolded Protein Response Signal Activator IRE1." *Frontiers in Molecular Biosciences* 6: 11.

Ait-Bouziad, N., G. Lv, A. L. Mahul-Mellier, et al. 2017. "Discovery and Characterization of Stable and Toxic Tau/Phospholipid Oligomeric Complexes." *Nature Communications* 8: 1678.

Ali, A., A. P. Holman, A. Rodriguez, M. Matveyenka, and D. Kurouski. 2024. "Tubulin-Binding Region Alters Tau-Lipid Interactions and Changes Toxicity of Tau Fibrils Formed in the Presence of Phosphatidylserine Lipids." *Protein Science* 33: e5078.

Ali, A., K. Zhaliazka, T. Dou, A. P. Holman, R. Kumar, and D. Kurouski. 2023. "Secondary Structure and Toxicity of Transthyretin Fibrils Can Be Altered by Unsaturated Fatty Acids." *International Journal of Biological Macromolecules* 253: 127241.

Ali, A., K. Zhaliazka, T. Dou, A. P. Holman, and D. Kurouski. 2023a. "Cholesterol and Sphingomyelin Uniquely Alter the Rate of Transthyretin Aggregation and Decrease the Toxicity of Amyloid Fibrils." *Journal of Physical Chemistry Letters* 14: 10886–10893.

Ali, A., K. Zhaliazka, T. Dou, A. P. Holman, and D. Kurouski. 2023b. "Role of Saturation and Length of Fatty Acids of Phosphatidylserine in the Aggregation of Transthyretin." *ACS Chemical Neuroscience* 14: 3499–3506.

Ali, A., K. Zhaliazka, T. Dou, A. P. Holman, and D. Kurouski. 2023c. "Saturation of Fatty Acids in Phosphatidic Acid Uniquely Alters Transthyretin Stability Changing Morphology and Toxicity of Amyloid Fibrils." *Chemistry and Physics of Lipids* 257: 105350.

Ali, A., K. Zhaliazka, T. Dou, A. P. Holman, and D. Kurouski. 2023d. "The Toxicities of A30P and A53T Alpha-Synuclein Fibrils Can Be Uniquely Altered by the Length and Saturation of Fatty Acids in Phosphatidylserine." *Journal of Biological Chemistry* 299: 105383.

Alonso, A. D., T. Zaidi, M. Novak, H. S. Barra, I. Grundke-Iqbal, and K. Iqbal. 2001. "Interaction of Tau Isoforms With Alzheimer's Disease Abnormally Hyperphosphorylated Tau and In Vitro Phosphorylation Into the Disease-Like Protein." *Journal of Biological Chemistry* 276: 37967–37973.

Alonso Adel, C., A. Mederlyova, M. Novak, I. Grundke-Iqbal, and K. Iqbal. 2004. "Promotion of Hyperphosphorylation by Frontotemporal Dementia Tau Mutations." *Journal of Biological Chemistry* 279: 34873–34881.

Asai, H., S. Ikezu, S. Tsunoda, et al. 2015. "Depletion of Microglia and Inhibition of Exosome Synthesis Halt Tau Propagation." *Nature Neuroscience* 18: 1584–1593.

Bertolotti, A., Y. Zhang, L. M. Hendershot, H. P. Harding, and D. Ron. 2000. "Dynamic Interaction of BiP and ER Stress Transducers in the Unfolded-Protein Response." *Nature Cell Biology* 2: 326–332.

Calfon, M., H. Zeng, F. Urano, et al. 2002. "IRE1 Couples Endoplasmic Reticulum Load to Secretory Capacity by Processing the XBP-1 mRNA." *Nature* 415: 92–96.

Clavaguera, F., T. Bolmont, R. A. Crowther, et al. 2009. "Transmission and Spreading of Tauopathy in Transgenic Mouse Brain." *Nature Cell Biology* 11: 909–913.

Dicke, S. S., L. Tatge, P. E. Engen, M. Culp, and L. R. Masterson. 2017. "Isothermal Titration Calorimetry and Vesicle Leakage Assays Highlight the Differential Behaviors of Tau Repeat Segments Upon Interaction With Anionic Lipid Membranes." *Biochemical and Biophysical Research Communications* 493: 1504–1509.

Dou, T., and D. Kurouski. 2022. "Phosphatidylcholine and Phosphatidylserine Uniquely Modify the Secondary Structure of Alpha-Synuclein Oligomers Formed in Their Presence at the Early Stages of Protein Aggregation." *ACS Chemical Neuroscience* 13: 2380–2385.

Dou, T., M. Matveyenka, and D. Kurouski. 2023. "Elucidation of Secondary Structure and Toxicity of Alpha-Synuclein Oligomers and Fibrils Grown in the Presence of Phosphatidylcholine and Phosphatidylserine." *ACS Chemical Neuroscience* 14: 3183–3191.

Eisenberg, D. S., and M. R. Sawaya. 2017. "Neurodegeneration: Taming Tangled Tau." *Nature* 547: 170–171.

El Mammeri, N., O. Gampp, P. Duan, and M. Hong. 2023. "Membrane-Induced Tau Amyloid Fibrils." *Communications Biology* 6: 467.

Elbaum-Garfinkle, S., T. Ramlall, and E. Rhoades. 2010. "The Role of the Lipid Bilayer in Tau Aggregation." *Biophysical Journal* 98: 2722–2730.

Falcon, B., J. Zivanov, W. Zhang, et al. 2019. "Novel Tau Filament Fold in Chronic Traumatic Encephalopathy Encloses Hydrophobic Molecules." *Nature* 568: 420–423.

Gerson, J., D. L. Castillo-Carranza, U. Sengupta, et al. 2016. "Tau Oligomers Derived From Traumatic Brain Injury Cause Cognitive Impairment and Accelerate Onset of Pathology in Htau Mice." *Journal of Neurotrauma* 33: 2034–2043.

Giamblanco, N., Y. Fichou, J. M. Janot, E. Balanzat, S. Han, and S. Balme. 2020. "Mechanisms of Heparin-Induced Tau Aggregation Revealed by a Single Nanopore." *ACS Sensors* 5: 1158–1167.

Goedert, M., M. G. Spillantini, R. Jakes, D. Rutherford, and R. A. Crowther. 1989. "Multiple Isoforms of Human Microtubule-Associated Protein Tau: Sequences and Localization in Neurofibrillary Tangles of Alzheimer's Disease." *Neuron* 3: 519–526.

Gouras, G. K., D. Tampellini, R. H. Takahashi, and E. Capetillo-Zarate. 2010. "Intraneuronal Beta-Amyloid Accumulation and Synapse Pathology in Alzheimer's Disease." *Acta Neuropathologica* 119: 523–541.

Grundke-Iqbal, I., K. Iqbal, Y. C. Tung, M. Quinlan, H. M. Wisniewski, and L. I. Binder. 1986. "Abnormal Phosphorylation of the Microtubule-Associated Protein Tau (Tau) in Alzheimer Cytoskeletal Pathology." *Proceedings of the National Academy of Sciences of the United States of America* 83: 4913–4917.

Harding, H. P., Y. Zhang, A. Bertolotti, H. Zeng, and D. Ron. 2000. "Perk Is Essential for Translational Regulation and Cell Survival During the Unfolded Protein Response." *Molecular Cell* 5: 897–904.

Harding, H. P., Y. Zhang, and D. Ron. 1999. "Protein Translation and Folding Are Coupled by an Endoplasmic-Reticulum-Resident Kinase." *Nature* 397: 271–274.

Himmler, A., D. Drechsel, M. W. Kirschner, and D. W. Martin Jr. 1989. "Tau Consists of a Set of Proteins With Repeated C-Terminal Microtubule-Binding Domains and Variable N-Terminal Domains." *Molecular and Cellular Biology* 9: 1381–1388.

Hoshi, M., M. Sato, S. Matsumoto, et al. 2003. "Spherical Aggregates of Beta-Amyloid (Amylospheroid) Show High Neurotoxicity and Activate Tau Protein Kinase I/Glycogen Synthase Kinase-3beta." *Proceedings of the National Academy of Sciences of the United States of America* 100: 6370–6375.

Iwakoshi, N. N., A. H. Lee, and L. H. Glimcher. 2003. "The X-Box Binding Protein-1 Transcription Factor Is Required for Plasma Cell Differentiation and the Unfolded Protein Response." *Immunological Reviews* 194: 29–38.

Jakubec, M., E. Barias, S. Furse, et al. 2021. "Cholesterol-Containing Lipid Nanodiscs Promote an Alpha-Synuclein Binding Mode That Accelerates Oligomerization." *FEBS Journal* 288: 1887–1905.

Karikari, T. K., D. A. Nagel, A. Grainger, C. Clarke-Bland, E. J. Hill, and K. G. Moffat. 2019. "Preparation of Stable Tau Oligomers for Cellular and Biochemical Studies." *Analytical Biochemistry* 566: 67–74.

Kondow-McConaghy, H. M., N. Muthukrishnan, A. Erazo-Oliveras, K. Najjar, R. L. Juliano, and J. P. Pellois. 2020. "Impact of the Endosomal Escape Activity of Cell-Penetrating Peptides on the Endocytic Pathway." *ACS Chemical Biology* 15: 2355–2363.

Kopp, M. C., N. Larburu, V. Durairaj, C. J. Adams, and M. M. U. Ali. 2019. "UPR Proteins IRE1 and PERK Switch BiP From Chaperone to ER Stress Sensor." *Nature Structural & Molecular Biology* 26: 1053–1062.

Kurouski, D. 2023. "Elucidating the Role of Lipids in the Aggregation of Amyloidogenic Proteins." *Accounts of Chemical Research* 56: 2898–2906.

LaPointe, N. E., G. Morfini, G. Pigino, et al. 2009. "The Amino Terminus of Tau Inhibits Kinesin-Dependent Axonal Transport: Implications for Filament Toxicity." *Journal of Neuroscience Research* 87: 440–451.

Lasagna-Reeves, C. A., D. L. Castillo-Carranza, G. R. Jackson, and R. Kayed. 2011. "Tau Oligomers as Potential Targets for Immunotherapy for Alzheimer's Disease and Tauopathies." *Current Alzheimer Research* 8: 659–665.

Lasagna-Reeves, C. A., D. L. Castillo-Carranza, U. Sengupta, A. L. Clos, G. R. Jackson, and R. Kayed. 2011. "Tau Oligomers Impair Memory and Induce Synaptic and Mitochondrial Dysfunction in Wild-Type Mice." *Molecular Neurodegeneration* 6: 39.

Lasagna-Reeves, C. A., D. L. Castillo-Carranza, U. Sengupta, et al. 2012a. "Alzheimer Brain-Derived Tau Oligomers Propagate Pathology From Endogenous Tau." *Scientific Reports* 2: 700.

Lasagna-Reeves, C. A., D. L. Castillo-Carranza, U. Sengupta, et al. 2012b. "Identification of Oligomers at Early Stages of Tau Aggregation in Alzheimer's Disease." *FASEB Journal* 26: 1946–1959.

Lee, A. H., N. N. Iwakoshi, K. C. Anderson, and L. H. Glimcher. 2003. "Proteasome Inhibitors Disrupt the Unfolded Protein Response in Myeloma Cells." *Proceedings of the National Academy of Sciences of the United States of America* 100: 9946–9951.

Lee, A. H., N. N. Iwakoshi, and L. H. Glimcher. 2003. "XBP-1 Regulates a Subset of Endoplasmic Reticulum Resident Chaperone Genes in the Unfolded Protein Response." *Molecular and Cellular Biology* 23: 7448–7459.

Matveyenka, M., S. Rizevsky, and D. Kurouski. 2022. "Amyloid Aggregates Exert Cell Toxicity Causing Irreversible Damages in the Endoplasmic Reticulum." *Biochimica et Biophysica Acta, Molecular Basis of Disease* 1868: 166485.

Matveyenka, M., S. Rizevsky, J. P. Pellois, and D. Kurouski. 2023. "Lipids Uniquely Alter Rates of Insulin Aggregation and Lower Toxicity of Amyloid Aggregates." *Biochimica et Biophysica Acta – Molecular and Cell Biology of Lipids* 1868: 159247.

Matveyenka, M., K. Zhaliazka, and D. Kurouski. 2024. "Macrophages and Natural Killers Degrade Alpha-Synuclein Aggregates." *Molecular Pharmaceutics* 21: 2565–2576.

Matveyenka, M., K. Zhaliazka, S. Rizevsky, and D. Kurouski. 2022. "Lipids Uniquely Alter Secondary Structure and Toxicity of Lysozyme Aggregates." *FASEB Journal* 36: e22543.

McLean, C. A., R. A. Cherny, F. W. Fraser, et al. 1999. "Soluble Pool of Abeta Amyloid as a Determinant of Severity of Neurodegeneration in Alzheimer's Disease." *Annals of Neurology* 46: 860–866.

Medina, D. L., S. Di Paola, I. Peluso, et al. 2015. "Lysosomal Calcium Signalling Regulates Autophagy Through Calcineurin and TFEB." *Nature Cell Biology* 17: 288–299.

Morfini, G. A., M. Burns, L. I. Binder, et al. 2009. "Axonal Transport Defects in Neurodegenerative Diseases." *Journal of Neuroscience* 29: 12776–12786.

Nath, S., L. Agholme, F. R. Kurudenkandy, B. Granseth, J. Marcusson, and M. Hallbeck. 2012. "Spreading of Neurodegenerative Pathology via Neuron-To-Neuron Transmission of Beta-Amyloid." *Journal of Neuroscience* 32: 8767–8777.

Oslowski, C. M., and F. Urano. 2011. "The Binary Switch That Controls the Life and Death Decisions of ER Stressed Beta Cells." *Current Opinion in Cell Biology* 23: 207–215.

Radulovic, M., K. O. Schink, E. M. Wenzel, et al. 2018. "ESCRT-Mediated Lysosome Repair Precedes Lysophagy and Promotes Cell Survival." *EMBO Journal* 37: e99753.

Rajendran, L., M. Honsho, T. R. Zahn, et al. 2006. "Alzheimer's Disease Beta-Amyloid Peptides Are Released in Association With Exosomes." *Proceedings of the National Academy of Sciences of the United States of America* 103: 11172–11177.

Sallaberry, C. A., B. J. Voss, J. Majewski, et al. 2021. "Tau and Membranes: Interactions That Promote Folding and Condensation." *Frontiers in Cell and Development Biology* 9: 725241.

Sardiello, M., M. Palmieri, A. di Ronza, et al. 2009. "A Gene Network Regulating Lysosomal Biogenesis and Function." *Science* 325: 473–477.

Settembre, C., C. Di Malta, V. A. Polito, et al. 2011. "TFEB Links Autophagy to Lysosomal Biogenesis." *Science* 332: 1429–1433.

Shafiei, S. S., M. J. Guerrero-Munoz, and D. L. Castillo-Carranza. 2017. "Tau Oligomers: Cytotoxicity, Propagation, and Mitochondrial Damage." *Frontiers in Aging Neuroscience* 9: 83.

Shen, X., R. E. Ellis, K. Lee, et al. 2001. "Complementary Signaling Pathways Regulate the Unfolded Protein Response and Are Required for *C. elegans* Development." *Cell* 107: 893–903.

Skowyra, M. L., P. H. Schlesinger, T. V. Naismith, and P. I. Hanson. 2018. "Triggered Recruitment of ESCRT Machinery Promotes Endolysosomal Repair." *Science* 360: eaar5078.

Takashima, A. 2013. "Tauopathies and Tau Oligomers." *Journal of Alzheimer's Disease* 37: 565–568.

Urano, F., A. Bertolotti, and D. Ron. 2000. "IRE1 and Efferent Signaling From the Endoplasmic Reticulum." *Journal of Cell Science* 113, no. Pt 21: 3697–3702.

Wang, Y., V. Balaji, S. Kaniyappan, et al. 2017. "The Release and Trans-Synaptic Transmission of Tau via Exosomes." *Molecular Neurodegeneration* 12: 5.

Wegmann, S., B. Eftekharzadeh, K. Tepper, et al. 2018. "Tau Protein Liquid–Liquid Phase Separation Can Initiate Tau Aggregation." *EMBO Journal* 37: e98049.

Weingarten, M. D., A. H. Lockwood, S. Y. Hwo, and M. W. Kirschner. 1975. "A Protein Factor Essential for Microtubule Assembly." *Proceedings of the National Academy of Sciences of the United States of America* 72: 1858–1862.

Yao, Q. Q., J. Wen, S. Perrett, and S. Wu. 2022. "Distinct Lipid Membrane-Mediated Pathways of Tau Assembly Revealed by Single-Molecule Analysis." *Nanoscale* 14: 4604–4613.

Yoshiyama, Y., M. Higuchi, B. Zhang, et al. 2007. "Synapse Loss and Microglial Activation Precede Tangles in a P301S Tauopathy Mouse Model." *Neuron* 53: 337–351.

Zempel, H., E. Thies, E. Mandelkow, and E. M. Mandelkow. 2010. "Abeta Oligomers Cause Localized Ca(2+) Elevation, Missorting of Endogenous Tau Into Dendrites, Tau Phosphorylation, and Destruction of Microtubules and Spines." *Journal of Neuroscience* 30: 11938–11950.

Zhaliazka, K., A. Ali, and D. Kurouski. 2024. "Phospholipids and Cholesterol Determine Molecular Mechanisms of Cytotoxicity of Alpha-Synuclein Oligomers and Fibrils." *ACS Chemical Neuroscience* 15: 371–381.

Zhaliazka, K., M. Matveyenka, and D. Kurouski. 2023. "Lipids Uniquely Alter the Secondary Structure and Toxicity of Amyloid Beta 1-42 Aggregates." *FEBS Journal* 290: 3203–3220.

Zhang, W., B. Falcon, A. G. Murzin, et al. 2019. "Heparin-Induced Tau Filaments Are Polymorphic and Differ From Those in Alzheimer's and Pick's Diseases." *eLife* 8: e43584.

Supporting Information

Additional supporting information can be found online in the Supporting Information section.